molecules

MDPI

Review

Insights into Layered Oxide Cathodes for Rechargeable Batteries

Julia H. Yang [1], Haegyeom Kim [2] and Gerbrand Ceder [1,2,*]

[1] Department of Materials Science and Engineering, UC Berkeley, Berkeley, CA 94720, USA; juliayang@berkeley.edu
[2] Materials Sciences Division, Lawrence Berkeley National Laboratory, Berkeley, CA 94720, USA; haegyumkim@lbl.gov
* Correspondence: gceder@berkeley.edu

Abstract: Layered intercalation compounds are the dominant cathode materials for rechargeable Li-ion batteries. In this article we summarize in a pedagogical way our work in understanding how the structure's topology, electronic structure, and chemistry interact to determine its electrochemical performance. We discuss how alkali–alkali interactions within the Li layer influence the voltage profile, the role of the transition metal electronic structure in dictating O3-structural stability, and the mechanism for alkali diffusion. We then briefly delve into emerging, next-generation Li-ion cathodes that move beyond layered intercalation hosts by discussing disordered rocksalt Li-excess structures, a class of materials which may be essential in circumventing impending resource limitations in our era of clean energy technology.

Keywords: layered oxide cathodes; alkali–alkali interactions; electronic structure; Li diffusion

Citation: Yang, J.H.; Kim, H.; Ceder, G. Insights into Layered Oxide Cathodes for Rechargeable Batteries. *Molecules* **2021**, *26*, 3173. https://doi.org/10.3390/molecules26113173

Academic Editors: Stephane Jobic, Claude Delmas and Myung-Hwan Whangbo

Received: 2 May 2021
Accepted: 24 May 2021
Published: 26 May 2021

1. Introduction to the O3 Structure

Rechargeable Li-ion batteries have enabled a wireless revolution and are currently the dominant technology used to power electric vehicles and provide resilience to a grid powered by renewables. Research in the 1970s to create superconductors by modifying the carrier density of chalcogenides through intercalation [1] transitioned into energy storage when Whittingham demonstrated in 1976 a rechargeable battery using the layered TiS_2 cathode and Li metal anode [2]. Soon thereafter, Mizushima, Jones, Wiseman, and Goodenough demonstrated that a much higher voltage could be achieved by reversible Li de-intercalation from layered $LiCoO_2$ [3], energizing generations of rechargeable battery research. In this short review we revisit our work in understanding a few basic relationships between the structure, electronic structure, and properties of layered cathode materials.

A layered rocksalt cathode oxide adopts the general formula A_xMO_2 (A: alkali cation, M: metal cation, O: oxygen anion). The O anions form a face-centered cubic (FCC) framework with octahedral and tetrahedral sites. These two environments are face sharing and form a topologically connected network. When fully alkaliated such that x ~ 1, the compound consists of AO_2 and MO_2 edge-sharing octahedra. The layered structure, illustrated in Figure 1, is aptly named because AO_2/MO_2 octahedra form alternating (111) planes of the FCC oxygen lattice when fully lithiated. The A and M cations alternate in the abc repeat unit of the oxygen framework to form a−b_c−a_b−c_, stacking where the minus sign "−" indicates the location of M and the underscore "_" gives the position of the A ions. Because the oxygen stacking has a repeat unit of three and the metal layering repeats every two layers, periodicity is achieved after six oxygen layers. Under the structural classification by Delmas et al. for layered cathode oxides [4], the layered rocksalt cathode structure is commonly referred to as O3: O for the octahedral alkali ion environment (not to be confused with O for oxygen) and 3 for the number of MO_2 slabs in a repeat unit. The

O3 structure is equivalent to the structure of α-$NaFeO_2$ and the cation ordering is also known in metallic alloys as $L1_1$ (CuPt prototype) [5].

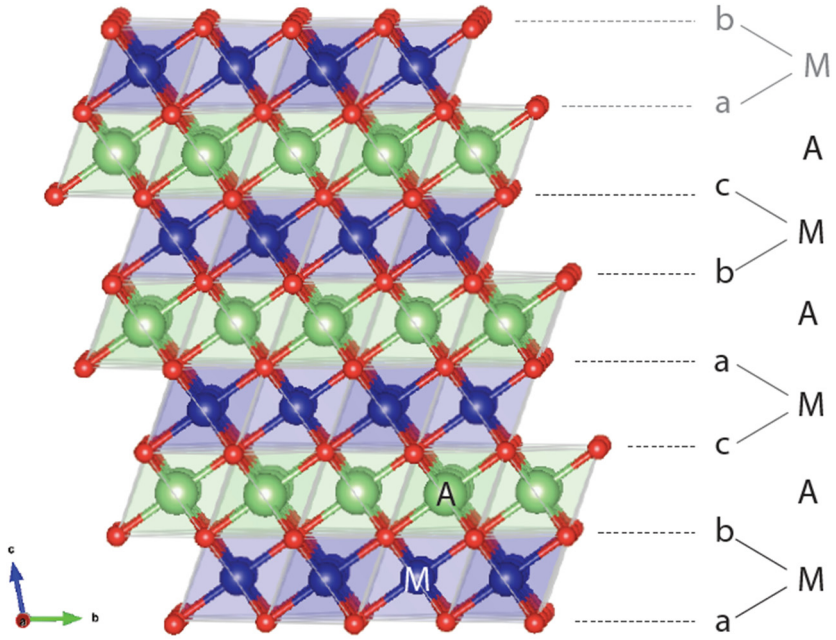

Figure 1. Representative O3 structure showing the abc stacking sequence of oxygen ions (red), thus creating various coordination environments for the alkali ion A (green) and metal ion M (blue). In an O3 repeat unit, M and A are coordinated below and above by oxygen layers. The beginning of another repeat unit with a-M-b stacking is in gray.

It is now well understood that the ordering of AO_2 and MO_2 in alternating layers is not the most favored cation ordering from an electrostatic perspective. Instead, the layered structure finds its stability in the size difference of A and M [6,7] as it allows A-O and M-O bond distances to relax independently of each other. This independent A-O and M-O bond accommodation explains how a larger A cation, such as Na^+, can form the layered structure with a wide range of M radii [8], whereas a smaller A, such as Li^+, only forms stable O3 compounds with a limited range of smaller M radii, namely Co^{3+} [9], V^{3+} [10], Ni^{3+} [11], and Cr^{3+} [10].

2. Evolution from $LiCoO_2$ to NMC

Today, O3 cathodes have evolved in several directions from $LiCoO_2$ [12] for use cases beyond portable electronics. Anticipating potential cost and resource problems with Co [13], research in the 1980s and 1990s mostly focused on substitutions of Co by Ni [14]. However, consideration of the low cost of Mn and the high stability of the Mn^{4+} charge state led the community towards layered $LiMnO_2$. Even though this structure is not the thermodynamically stable state of $LiMnO_2$ [15], Delmas [16] and Bruce [17] were able to synthesize it by ion exchange from the stable $NaMnO_2$. Unfortunately, the high mobility of Mn^{3+} [18] leads to a rapid transformation of the layered structure into the spinel structure upon cycling [19] because of its pronounced energetic preference at the $Li_{0.5}MnO_2$ composition [20]. Attempts to stabilize layered $LiMnO_2$ with Al [21] or Cr [22,23] substitution were only partially successful and led to the formation of a phase intermediate between layered and spinel [24]. Then, in 2001, several key papers were published that would pave the way for the highly successful Ni-Mn-Co (NMC) cathode series: Ohzuku showed very high capacity and cyclability in $Li(Ni_{1/3}Mn_{1/3}Co_{1/3})O_2$ [25], known as NMC-111, and in $Li(Ni_{1/2}Mn_{1/2})O_2$ [26]; Lu and Dahn published their work on the $Li(Ni_xCo_{1-2x}Mn_x)O_2$ [27] and its Co-free Li-excess version $Li(Ni_xLi_{1/3-2/x}Mn_{2/3-x/3})O_2$ [28]. In these compounds Ni is valence +2 and Mn is +4 [29], thereby stabilizing the layered material against Mn

migration and providing double redox from Ni^{2+}/Ni^{4+}. At this point the NMC cathode series was born. Since then, Ni-rich NMC cathodes have become of great interest to both academia and industry because they deliver a capacity approaching 200 mAh/g and demonstrate high energy density, good rate capability, and moderate cost [30–32].

In this short article, we summarize some general and fundamental understanding we have gained in layered oxide cathodes, without delving into issues with very specific compositions. We focus on the roles of the alkali–alkali interaction, electronic structure, and alkali diffusion, and illustrate how these fundamental features conspire to control the electrochemical behavior of O3-structured layered oxides.

3. Alkali–Alkali Interactions, Alkali/Vacancy Ordering, and Voltage Slope

The voltage of a cathode compound is set by the chemical potential of its alkali ions [33] which itself is the derivative of the free energy with respect to alkali concentration. This thermodynamic connection between voltage and free energy creates a direct relation between the voltage profile, the alkali–alkali interactions, and phase transformations as functions of alkali content. While Na_xMO_2 compounds show many changes in the stacking of the oxygen host layers when the Na content is changed, phase transitions in Li_xMO_2 materials are mostly driven by the Li-vacancy configurational free energy, resulting from Li^+-Li^+ interactions in the layer [20,34]. In layered compounds with a single transition metal, such as Li_xCoO_2 and Li_xNiO_2, such phase transitions are easily observed as voltage plateaus and steps in the electrochemical charge–discharge profiles as shown in Figure 2a. For a first-order phase transformation, for example from Phase I to Phase II, the Gibbs phase rule dictates that the Li chemical potential should be constant, hence the voltage remains constant while one phase transforms into the other. Phases in which the alkali ions are well-ordered usually display a rapid voltage change as the alkali content is changed, reflecting the high energy cost of trying to create off-stoichiometry in ordered phases. This is in contrast to solid solutions which have smoother voltage profiles as a function of alkali concentration. For example, both theory [35] and experiments [36,37] indicate that in Li_xCoO_2 a monoclinic phase appears with lithium and vacancies ordered in rows for $x \approx 0.5$ [36]. In Li_xNiO_2, Li-vacancy ordering is responsible for stable phases at $x \sim 0.8$, ~0.5, and ~0.25–0.3 [38–40]. When many transition metals are mixed, as in NMC cathodes, the Li^+-Li^+ interaction remains present, but Li-vacancy ordering is suppressed by the electrostatic and elastic perturbations on the Li site caused by the distribution of the Ni, Mn and Co in the transition metal layers.

The Li^+-Li^+ interaction is mostly electrostatic but is highly screened by the charge density on the oxygen ions, leading to a rather small effective interaction in layered Li_xMO_2 compounds and small voltage slope. This is a critical feature of Li_xMO_2 compounds that gives them high capacity in a relatively narrow voltage window compared to other alkali compounds, as explained below. The effective interaction between intercalating ions increases significantly when larger alkali ions (e.g., Na^+ and K^+) are used in the layered structure [41–43]. These larger alkali ions increase the oxygen slab distance, reducing the oxygen charge density available for screening within the alkali layer [20,42,43]. The larger effective repulsion between the Na^+ or K^+ ions affects the phase transition and electrochemistry in a very significant way as shown in Figure 2b. For example, Na_xCoO_2 has stronger Na-vacancy ordering and thus more pronounced voltage steps compared to Li_xCoO_2. This phenomenon [44,45] becomes even more significant in K_xCoO_2 [46,47]. The effect of the intercalant's size on the phase transitions and voltage steps is not just limited to Co-containing compounds but is also generally applicable to other transition metal systems as described in a recent review [43].

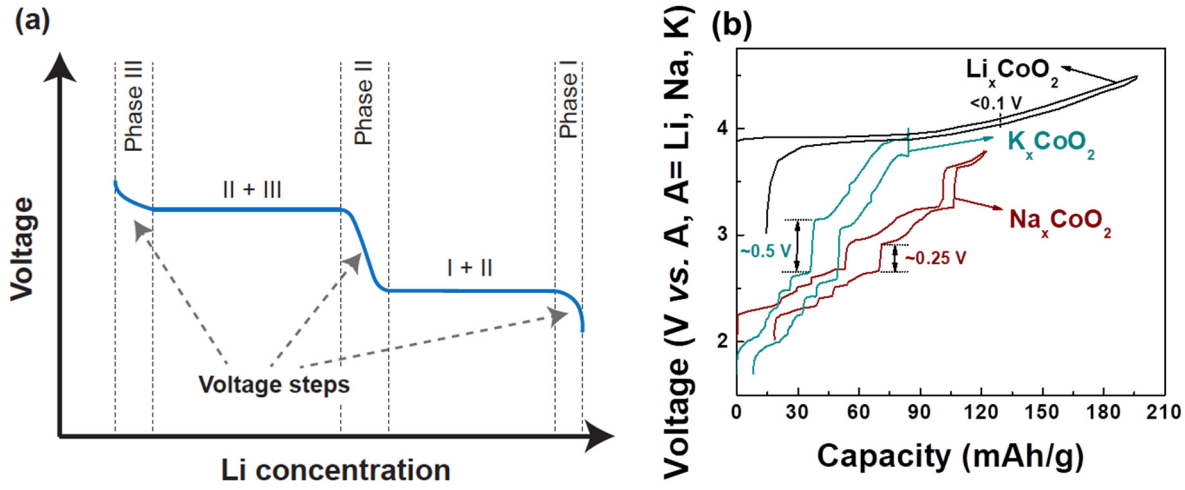

Figure 2. (**a**) Typical charge–discharge of intercalation-based cathode materials. A voltage step indicates new phase formation. (**b**) Charge–discharge comparison of O3-Li_xCoO_2, P2-Na_xCoO_2, and P2-K_xCoO_2 [44,47,48]. Voltage curves for P2-Na_xCoO_2, P2-K_xCoO_2, and O3-Li_xCoO_2 are reproduced with permissions from [44,47,48]. The voltage curve for P2-K_xCoO_2 is licensed under CC BY-NC 4.0 [47].

In practice, the larger effective interaction between alkali ions in the layered transition metal oxides is detrimental for their electrochemical performance. First, more phase transitions are likely to induce more mechanical stress in the cathode structure during charging and discharging, causing possible fracture of electrode particles. Second, a simple argument shows that the average voltage slope is proportional to the effective interaction: V(x) is equal to $-\mu_{Li}(x)$, and since $\mu_{Li}(x) = \frac{\partial G}{\partial x}$, $\frac{\partial V}{\partial x} = -\frac{\partial^2 G}{\partial x^2}$. In a simple regular solution model for mixing, this second derivative of the free energy is proportional to the effective interaction [41,43,49]. Hence, when the effective interaction is large, as in layered K_xMO_2 compounds, the voltage curve has a high slope, limiting the achievable capacity between fixed voltage limits. This analysis shows that the advantage of lithium systems in providing large capacity within reasonable voltage limits is in part due to the highly effective screening of the Li^+-Li^+ interaction by oxygen. For Na, and in particular for K-ion based intercalation energy storage, it may be more advantageous to search among poly-anion compounds for good cathodes [43].

4. Electronic Structure of $LiCoO_2$

The electronic structure of layered $LiMO_2$ oxides is well understood. Due to the large energy difference in electronic levels between Li and the transition metal (TM), their electronic states do not mix and the behavior of the compound is controlled by the (MO_2) complex within which the transition metal and oxygen hybridize. In the R3-m symmetry of the layered structure, the environment of the TM is pseudo-octahedral in that all TM-O bond lengths are of equal length, but O-TM-O angles have small deviations from those in a perfect octahedron. The pseudo-octahedral symmetry splits the otherwise degenerate TM-*d* orbitals in three (lower energy) t_{2g} and two (higher energy) e_g orbitals yielding an energy separation called the octahedral ligand-field splitting, abbreviated as Δ_0. A more complete schematic of an orbital diagram is given in Figure 3a. The t_{2g} orbitals are shown as "non-bonding" in this schematic though in reality some π-hybridization takes place between them and the oxygen *p*-orbitals [50]. In the most basic picture in which one considers the overlap of the TM-*d* orbitals with its ligand *p*-states, the t_{2g} orbitals are formed from the d_{xy}-type *d*-orbitals which point away from ligands. In contrast, the d_{z2} and d_{x2-y2} orbitals of the TM point toward the ligand creating σ-overlap. The e_g* orbitals are the anti-bonding component of this hybridization and are dominated by TM states, whereas the bonding components, $e_g{}^b$, sit deep in the oxygen-dominated part of the band structure. Hybridization of the oxygen 2*p* and the metal 4*d* and 4*s* make up the remaining part of

the band structure. Because the e_g* orbitals result from σ-overlap between TM *d* states and oxygen *p*-states their energy is most sensitive to the TM-O bond length. Inducing, for example, a Jahn–Teller distortion moves these levels considerably. One can recover the characteristics of this molecular orbital diagram in a more realistic band structure and density of states computed with Density Functional Theory using the meta-GGA SCAN density functional approximation [51] as shown in Figure 3b for $LiCoO_2$. The elemental contributions are indicated by the color of the bands with green being oxygen and red the Co 3*d* states. The two e_g*-like bands above the Fermi level (solid line) have mixed Co and O contribution while the three t_{2g}-like bands below the Fermi level have more pure metal contribution. These three bands have a small bandwidth due to their non-bonding nature. The lowest six bands shown are the bands dominated by the oxygen states in green.

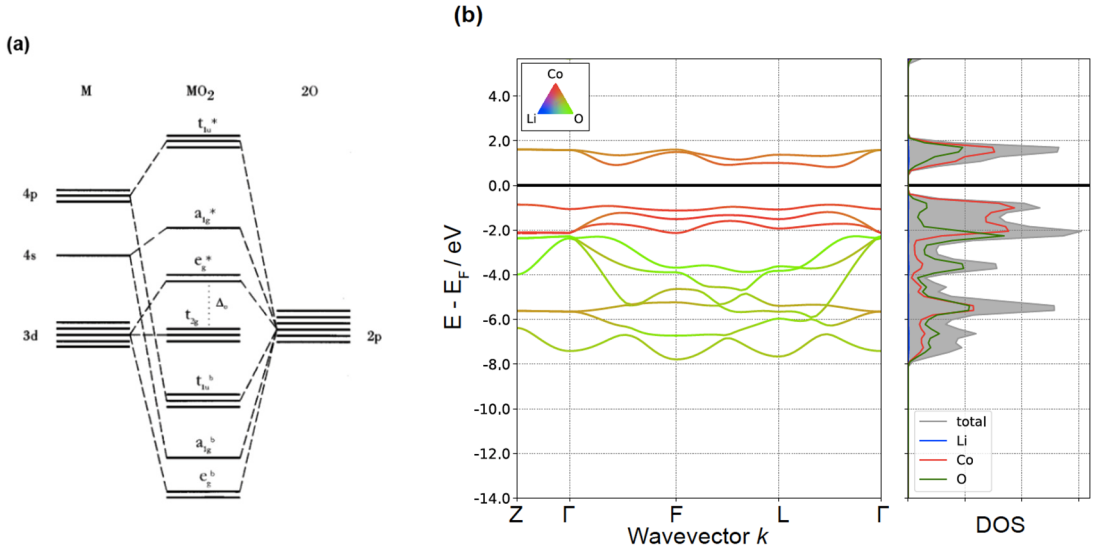

Figure 3. (**a**) The molecular orbital diagram for a $(MO_2)^-$ complex in octahedral environment. Reproduced with permission from [52]. (**b**) Calculated band structure and density of states with projections onto local orbitals for $LiCoO_2$, showing elemental contributions from Li (blue), Co (red), and O (green).

5. Electronic Structure Trends in Layered Li_xMO_2 Oxides

Because the ligand-induced splitting between transition metal *d* orbitals is fairly small, filling of states usually follows Hund's rule for creating high spin ions. Figure 4 illustrates this filling for 3*d* octahedral transition metal ions. Examples of this are Fe^{3+} (d^5) and Mn^{4+} (d^3). The high spin band filling implies that Mn^{3+} (d^4) and Fe^{4+} (d^4) with a single occupied e_g* state are Jahn–Teller active ions [50,53]. The later transition metals form exceptions to the high-spin rule in that Co^{3+} and Ni^{4+} are low-spin d^6 with all electrons occupying t_{2g} states. We discuss below that this is a key reason for their predominance as redox-active materials in layered oxides. The lack of any filled antibonding states in Co^{3+} makes this cation also one of the smallest 3*d* TM ions, which is reflected in the very high crystal density of $LiCoO_2$ of 5.051 g/cm^3 [54] and the associated high energy density. This electronic structure-induced high density makes $LiCoO_2$ still the preferred cathode material for portable electronics where battery volume comes at a high premium.

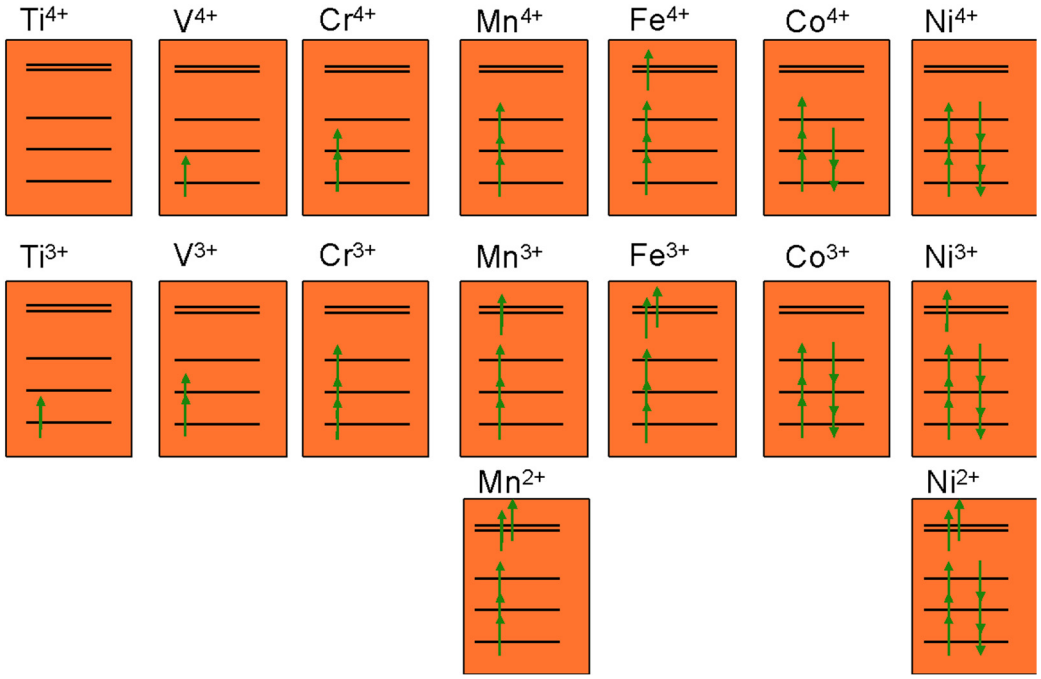

Figure 4. Expected transition metal band filling in the three t_{2g} and two e_g* states for 3*d* transition metals in octahedral environments.

Upon Li removal the hybridization of the orbitals changes. As an electron is removed from TM states the remaining TM *d* electrons experience less intra-atomic Coulombic repulsion and their states move down in energy, bringing them closer to the oxygen *p* states, resulting in increased hybridization. There are two notable consequences from this rehybridization [51,55]: (1) As hybridization transfers (filled) oxygen states onto the metal it increases the electron density on the metal site. Somewhat counterintuitively, almost no electron density change occurs on the metal after delithiation, even though it is formally oxidized, something that had been recognized earlier outside of the battery field in various Mn-oxides. This rehybridization by the anion explains why the anion has an almost larger influence on the voltage than the choice of 3*d* TM ion in layered compounds [52]. Effectively, the flexible hybridization between the TM and the O ligand creates a charge density buffer on the TM. (2) Covalency increases upon charging, leading in some cases to the fully charged material taking on the O1 (octahedral alkali environment with a repeat unit of 1 [4]) structure which is typically found in more covalent materials such as CdI_2. The increased covalency also sharply contracts the Li slab spacing (distance between the oxygen layers around the Li-layer) and *c*-lattice parameter when most of the alkali is removed [56].

6. Implications of Electronic Structure on Layered Stability

The orbital filling of the transition metals also plays a critical role in the stability of the layered structure upon Li removal. Ions with filled t_{2g} levels are most stable in the octahedral environment and resist any migration into the Li layer [57]. Because the oxygen arrangement is topologically equivalent to an FCC lattice, octahedral cation sites edge-share with each other and face-share with a tetrahedral site. Since ion migration through a shared edge comes with a very high energy barrier, cation diffusion between octahedral sites requires passage through an intermediate tetrahedral site. For ions with filled t_{2g} states, this passage through the tetrahedral site and the shared anion face raises the energy substantially as the octahedral ligand field stabilization is lost, making these ions all but immobile. In contrast, ions with d^5-high-spin (e.g., Mn^{2+} or Fe^{3+}) and d^0 filling (e.g., Ti^{4+}, V^{5+}) tend to be much more ambiguous about their preferred anion coordination, and as a result, tend to migrate more easily [57–59]. The most stable octahedral cations are

therefore low-spin-Co^{3+} (d^6) and low-spin-Ni^{4+} (d^6). In addition, high-spin-Mn^{4+} (d^3) also possesses very high octahedral stability as it adds Hund's rule coupling to the ligand field stabilization. These insights allow us to rationalize the prominence of the NMC class of layered oxides as cathodes in the Li-ion industry: Only Ni and Co have very high resistance against migration into the Li layer in the charged and discharged states. Mn^{4+} acts similarly, but cannot be used as a redox active element as its reduction or oxidation leads to an ion that is prone to migration [57,60,61]. Within the 3*d*-TM series there are unfortunately no other ions which can match the octahedral stability of the NMC chemistry, and layered oxides based on other *3d* TM are unlikely to be practical. Hence, it is the basic electronic structure of the 3*d* transition metal ions which is the direct cause of the serious resource problem the Li-ion industry faces if it wants to scale to multiple TWh annual production with layered oxides [13,62].

7. Diffusion Mechanism

In understanding alkali transport in layered compounds, and more generally in closed-packed oxides, it is important to assess how structure and chemistry influence performance, and ultimately, how one can design novel dense cathodes that are not layered. In this section, we focus on Li diffusion. Even though it is likely that Na and K migrate through a similar pathway, much less work has been done to validate the transport mechanism of these larger alkalis. The octahedral-tetrahedral-octahedral topology introduced earlier determines the diffusion mechanism in layered materials. Lithium migrates along the minimum energy path between two stable sites via an activated state, with the activation barrier defined as the difference between the maximum energy point along the path and the initial equilibrium position of the ion [63]. In layered Li_xCoO_2 [35], migration between neighboring octahedral sites can in principle occur through the shared octahedral edge formed by an oxygen–oxygen dumbbell (a mechanism referred to as an octahedral dumbbell hop (ODH)), or via the tetrahedral site that faces-shares with the initial and final octahedron (a tetrahedral site hop (TSH)). Figure 5 illustrates the ODH and TSH mechanisms in Li_xCoO_2.

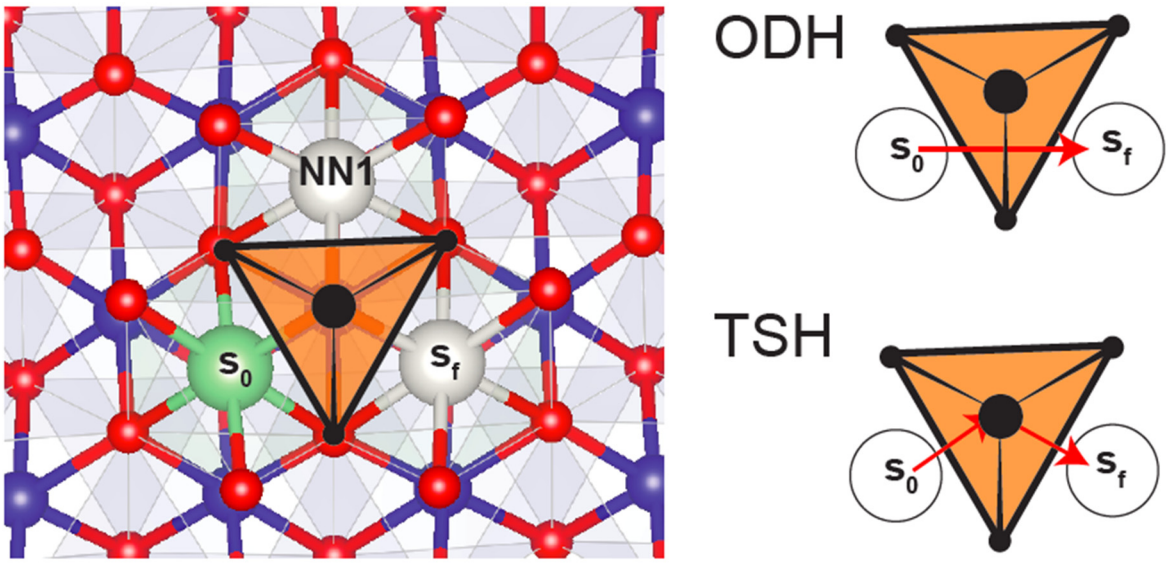

Figure 5. Li diffusion from site s_0 to s_f in layered materials. View of Li_xCoO_2 down the *c*-axis, with the top CoO_2 metal layer removed for clarity. The Li (green) layer and CoO_2 metal layer (Co: blue, O: red) below are shown. Black circles further indicate the O which coordinate the tetrahedral site colored in orange, showing how three of the tetrahedron faces are face-sharing with s_0, NN1, and s_f. The last face of the tetrahedron face-shares with Co in the metal layer below. Li in site s_0 can either diffuse from octahedral s_0 to octahedral s_f via the edge-sharing connection, thus completing an octahedral dumbbell hop (ODH) illustrated by the single red arrow, or through the empty tetrahedral site via the tetrahedral site hop (TSH) mechanism illustrated by the two red arrows. Site NN1 (white) is vacant.

A TSH requires the presence of a divacancy in the Li layer, which in Figure 5, implies that both s_f and NN1 need to be vacant. Van der Ven et al. used ab initio calculations to show that the ODH mechanism has a considerably higher activation barrier (~800 meV) than a TSH mechanism (230–600 meV) [63], establishing that Li diffusion in Li_xCoO_2 occurs predominantly by way of TSH for all practical lithiation levels. Even though the Li^+ in the activated state in the tetrahedron faces repulsion from a face-sharing $Co^{3+/4+}$ ion, the large Li slab spacing keeps the distance between Co and Li reasonable (Supplementary Materials).

The barrier for the TSH mechanism can vary from 230 to 600 meV due to local environment changes during lithiation. At x ~ 0.5, Li diffusion dips due to the ordering reaction [35] in agreement with experiment [36,64,65]. When a larger amount of Li (0.5 > x in Li_xCoO_2) is removed from the compound, a large decrease in the *c*-lattice parameter is observed experimentally and from first-principles [66–68]. Such lattice contraction increases the activation barrier significantly because it creates a smaller tetrahedron height and shorter distance between the activated Li^+ and the $Co^{3+/4+}$ ion. The larger positive charge on Co when the compound is more oxidized also contributes to an increase of the energy in the activated state. As a result, the activation barrier increases by hundreds of meV when delithiation increases past 0.5 Li [69]. While the precise behavior of the c-lattice parameter and slab spacing in NMC materials depends on the specific chemistry, the overall behavior is similar to $LiCoO_2$.

8. Beyond Layered Materials: DRX

It is now understood that the Li migration mechanism in layered oxides is a specific case of a more general framework for understanding ion transport in FCC close-packed oxides. Recent work [70,71] categorized the different environments that can occur around the tetrahedral activated state in close-packed oxides by the number of face-sharing transition metals it has. So-called *n*TM channels have *n* transition metals face-sharing, with the other face-sharing octahedral sites either occupied by Li or vacancies. Because minimally two Li (or vacant sites) are required to create a migration path, 4TM and 3TM channels do not participate in diffusion. Structures with only 2TM channels exist but display very poor Li mobility due to the large electrostatic repulsion Li^+ sees in the activated state from the two TM ions with which it face-shares. This theory explains why ordered γ-$LiFeO_2$, a compound with only 2TM channels, is not electrochemically active. Layered oxides contain 3TM and 1TM channels with Li diffusion occurring through the 1TM channels. However, the proximity of the TM to the Li^+ in a 1TM channel creates a strong dependence of the migration barrier on the size of the tetrahedron, which in layered materials is determined by the slab spacing. As shown extensively by Kang et al. [72,73], even small contractions of the slab spacing, caused by TM mixing in the Li layer, reduce Li mobility in a very substantial way. The "safest" migration paths are 0-TM channels: In the presence of a divacancy, a migrating Li^+ only electrostatically interacts with one other Li^+ ion making the activation energy rather insensitive to dimensional changes. Recent work has shown how to create cation-disordered materials in which transport occurs through these 0-TM channels [74]: When cations are fully disordered over the octahedral sites of a structure with FCC anion packing, all possible configurations around the activated state occur with some statistical probability, and percolation of the 0-TM channels into a macroscopic diffusion path occurs when more than 9% Li excess is present (i.e., x > 0.09 in $Li_{1+x}M_{1-x}O_2$). In reality, cation short-range order tends to reduce the amount of 0-TM channels from what would be in a random system [75] and a higher Li-excess content is needed or high-entropy ideas have to be applied to minimize short-range order [76]. Based on these insights, Li-excess rocksalt oxides with a disordered cation distribution have been shown to function as intercalation cathodes with high capacity [77]. Disordered Rocksalt Li-eXcess cathodes (DRX), also referred to as DRS (Disordered RockSalt) by some [78], do not require any specific ordering of the metal and Li cations, and can therefore be used with a broad range of redox active and non-redox active metals, alleviating the resource issue arising with

NMC layered cathodes. Indeed, almost all 3*d* and several 4*d* TM have been used as redox couples, including V^{4+}/V^{5+} and partial V^{3+}/V^{5+} [79], Mn^{2+}/Mn^{4+} [80], Mo^{3+}/Mo^{6+} [81], and partial Fe^{3+}/Fe^{4+} [82,83]. Redox-inactive d^0 TM elements, such as Ti^{4+}, V^{5+}, Nb^{5+}, and Mo^{6+} [77], play a particular role in DRX as they stabilize disorder [84], and their high valence compensates for excess Li content. Fluorination (anion substitution) is possible in DRX compounds which lowers the cation valence and extends cycle life by reducing oxygen redox [85]. Promising specific energies approaching 1000 Wh/kg (cathode only) have been achieved with Mn-Ti-based materials offering a possible low-cost, high-energy cathode solution for Li-ion.

9. Conclusions

The pioneering work of Professor Goodenough on $LiCoO_2$ [3] has led to a rich and widely used class of layered cathodes thereby transforming Li-ion into the leading energy storage technology for electronics, vehicles, and the grid. In this review, we discussed the topology of the layered structure and explain how the structure (1) sets the voltage slope trends among various alkali ions, (2) is critically limited to certain transition metals due to their electronic structure, and (3) controls the alkali diffusion mechanism. A 20-year effort to understand the phase stability, transport, and electronic structure in these compounds can now be broadened towards new high-energy density cathode materials, ensuring the future of Li-ion as an important contribution to clean energy technology.

Supplementary Materials: The following are available online. The supplemental information contains band structure calculation details.

Author Contributions: Writing—original draft preparation, J.H.Y., H.K., and G.C.; writing—reviewing and editing, J.H.Y., H.K. and G.C.; DFT-SCAN calculations, J.H.Y. and G.C. All authors have read and agreed to the published version of the manuscript.

Funding: This research received no additional funding.

Institutional Review Board Statement: Not applicable.

Informed Consent Statement: Not applicable.

Data Availability Statement: The $LiCoO_2$ structure used for calculating the band structure is freely available via the Materials Project database at https://materialsproject.org (accessed on 26 May 2021).

Acknowledgments: G.C. acknowledges long-term support from the Department of Energy, Office of Basic Energy Sciences, for the development of fundamental understanding of Li-intercalation cathodes. More recently, work on diffusion and on the development of DRX cathodes was supported by the Assistant Secretary for Energy Efficiency and Renewable Energy, Vehicle Technologies Office, under the Applied Battery Materials Program, of the U.S. Department of Energy under Contract No. DE-AC02-05CH11231, and under Contract No. DE-AC02-05CH11231, under the Advanced Battery Materials Research (BMR) Program.

Conflicts of Interest: The authors declare no conflict of interest.

References

1. Gamble, F.R.; Osiecki, J.H.; Cais, M.; Pisharody, R.; Disalvo, F.J.; Geballe, T.H. Intercalation complexes of lewis bases and layered sulfides: A large class of new superconductors. *Science* **1971**, *174*, 493–497. [CrossRef]
2. Whittingham, M.S. Electrical Energy Storage and Intercalation Chemistry. *Science* **1976**, *192*, 1126–1127. [CrossRef]
3. Mizushima, K.; Jones, P.C.; Wiseman, P.J.; Goodenough, J.B. $LixCoO_2$ ($0 < x < -1$): A new cathode material for batteries of high energy density. *Mater. Res. Bull.* **1980**, *15*, 783–789. [CrossRef]
4. Delmas, C.; Fouassier, C.; Hagenmuller, P. Structural classification and properties of the layered oxides. *Physica B+C* **1980**, *99*, 81–85. [CrossRef]
5. Ceder, G.; Van der Ven, A.; Marianetti, C.; Morgan, D. First-principles alloy theory in oxides. *Model. Simul. Mater. Sci. Eng.* **2000**, *8*, 311–321. [CrossRef]
6. Wu, E.J.; Tepesch, P.D.; Ceder, G. Size and charge effects on the structural stability of $LiMO_2$ (M = transition metal) compounds. *Philos. Mag. B* **1998**, *77*, 1039–1047. [CrossRef]

7. Hewston, T.A.; Chamberland, B.L. A Survey of first-row ternary oxides $LiMO_2$ (M = Sc-Cu). *J. Phys. Chem. Solids* **1987**, *48*, 97–108. [CrossRef]
8. Kim, S.; Ma, X.; Ong, S.P.; Ceder, G. A comparison of destabilization mechanisms of the layered Na_xMO_2 and Li_xMO_2 compounds upon alkali de-intercalation. *Phys. Chem. Chem. Phys.* **2012**, *14*, 15571–15578. [CrossRef] [PubMed]
9. Orman, H.J.; Wiseman, P.J. Cobalt(III) lithium oxide, $CoLiO_2$: Structure refinement by powder neutron diffraction. *Acta Crystallogr. Sect. C* **1984**, *40*, 12–14. [CrossRef]
10. Rüdorff, W.; Becker, H. Notizen: Die Strukturen von $LiVO_2$, $NaVO_2$, $LiCrO_2$ und $NaCrO_2$. *Z. Nat. B* **1954**, *9*, 614–615. [CrossRef]
11. Dyer, L.D.; Borie, B.S.; Smith, G.P. Alkali Metal-Nickel Oxides of the Type $MNiO_2$. *J. Am. Chem. Soc.* **1954**, *76*, 1499–1503. [CrossRef]
12. Manthiram, A.; Goodenough, J.B. Layered lithium cobalt oxide cathodes. *Nat. Energy* **2021**, *6*, 323. [CrossRef]
13. Fu, X.; Beatty, D.N.; Gaustad, G.G.; Ceder, G.; Roth, R.; Kirchain, R.E.; Olivetti, E.A. Perspectives on Cobalt Supply through 2030 in the Face of Changing Demand. *Environ. Sci. Technol.* **2020**, *54*, 2985–2993. [CrossRef] [PubMed]
14. Delmas, C.; Saadoune, I. Electrochemical and physical properties of the $Li_xNi_{1-y}Co_yO_2$ phases. *Solid State Ion.* **1992**, *53–56*, 370–375. [CrossRef]
15. Ceder, G. The Stability of Orthorhombic and Monoclinic-Layered $LiMnO_2$. *Electrochem. Solid-State Lett.* **1999**, *2*, 550. [CrossRef]
16. Capitaine, F.; Gravereau, P.; Delmas, C. A new variety of $LiMnO_2$ with a layered structure. *Solid State Ion.* **1996**, *89*, 197–202. [CrossRef]
17. Armstrong, A.R.; Bruce, P.G. Synthesis of layered $LiMnO_2$ as an electrode for rechargeable lithium batteries. *Nature* **1996**, *381*, 499–500. [CrossRef]
18. Reed, J.; Ceder, G.; Van Der Ven, A. Layered-to-Spinel Phase Transition in Li_xMnO_2. *Electrochem. Solid-State Lett.* **2001**, *4*, A78. [CrossRef]
19. Shao-Horn, Y.; Hackney, S.A.; Armstrong, A.R.; Bruce, P.G.; Gitzendanner, R.; Johnson, C.S.; Thackeray, M.M. Structural Characterization of Layered $LiMnO_2$ Electrodes by Electron Diffraction and Lattice Imaging. *J. Electrochem. Soc.* **1999**, *146*, 2404–2412. [CrossRef]
20. Ceder, G.; Van der Ven, A. Phase diagrams of lithium transition metal oxides: Investigations from first principles. *Electrochim. Acta* **1999**, *45*, 131–150. [CrossRef]
21. Jang, Y.; Huang, B.; Wang, H.; Sadoway, D.R.; Ceder, G.; Chiang, Y.; Liu, H.; Tamura, H. $LiAl_yCo_{1-y}O_2$ (R-3m) Intercalation Cathode for Rechargeable Lithium Batteries. *J. Electrochem. Soc.* **1999**, *146*, 862–868. [CrossRef]
22. Dahn, J.R.; Zheng, T.; Thomas, C.L. Structure and Electrochemistry of $Li_2Cr_xMn_{2-x}O_4$ for $1.0 \leq x \leq 1.5$. *J. Electrochem. Soc.* **1998**, *145*, 851–859. [CrossRef]
23. Davidson, I.J.; McMillan, R.S.; Murray, J.J.; Greedan, J.E. Lithium-ion cell based on orthorhombic $LiMnO_2$. *J. Power Sources* **1995**, *54*, 232–235. [CrossRef]
24. Reed, J.S. Ab-Initio Study of Cathode Materials for Lithium Batteries. Ph.D. Thesis, Massachusetts Institute of Technology, Cambridge, MA, USA, 2003.
25. Ohzuku, T.; Makimura, Y. Layered Lithium Insertion Material of $LiCo_{1/3}Ni_{1/3}Mn_{1/3}O_2$ for Lithium-Ion Batteries. *Chem. Lett.* **2001**, *30*, 642–643. [CrossRef]
26. Ohzuku, T.; Makimura, Y. Layered Lithium Insertion Material of $LiNi_{1/2}Mn_{1/2}O_2$: A Possible Alternative to $LiCoO_2$ for Advanced Lithium-Ion Batteries. *Chem. Lett.* **2001**, *30*, 744–745. [CrossRef]
27. Lu, Z.; MacNeil, D.D.; Dahn, J.R. Layered $Li[Ni_xCo_{1-2x}Mn_x]O_2$ Cathode Materials for Lithium-Ion Batteries. *Electrochem. Solid-State Lett.* **2001**, *4*, A200. [CrossRef]
28. Lu, Z.; MacNeil, D.D.; Dahn, J.R. Layered Cathode Materials $Li[Ni_xLi_{1/3-2x/3}Mn_{2/3-x/3}]O_2$ for Lithium-Ion Batteries. *Electrochem. Solid-State Lett.* **2001**, *4*, A191. [CrossRef]
29. Reed, J.; Ceder, G. Charge, Potential, and Phase Stability of Layered $Li(Ni_{0.5}Mn_{0.5})O_2$. *Electrochem. Solid-State Lett.* **2002**, *5*, A145. [CrossRef]
30. Manthiram, A.; Song, B.; Li, W. A perspective on nickel-rich layered oxide cathodes for lithium-ion batteries. *Energy Storage Mater.* **2017**, *6*, 125–139. [CrossRef]
31. Kim, J.; Lee, H.; Cha, H.; Yoon, M.; Park, M.; Cho, J. Prospect and Reality of Ni-Rich Cathode for Commercialization. *Adv. Energy Mater.* **2018**, *8*, 1702028. [CrossRef]
32. Zhu, L.; Bao, C.; Xie, L.; Yang, X.; Cao, X. Review of synthesis and structural optimization of $LiNi_{1/3}Co_{1/3}Mn_{1/3}O_2$ cathode materials for lithium-ion batteries applications. *J. Alloys Compd.* **2020**, *831*, 154864. [CrossRef]
33. Aydinol, M.K.; Ceder, G. First-Principles Prediction of Insertion Potentials in Li-Mn Oxides for Secondary Li Batteries. *J. Electrochem. Soc.* **1997**, *144*, 3832–3835. [CrossRef]
34. Li, W.; Reimers, J.N.; Dahn, J.R. Lattice-gas-model approach to understanding the structures of lithium transition-metal oxides $LiMO_2$. *Phys. Rev. B* **1994**, *49*, 826–831. [CrossRef] [PubMed]
35. Van der Ven, A.; Aydinol, M.K.; Ceder, G.; Kresse, G.; Hafner, J. First-principles investigation of phase stability in Li_xCoO_2. *Phys. Rev. B* **1998**, *58*, 2975–2987. [CrossRef]
36. Reimers, J.N.; Dahn, J.R. Electrochemical and In Situ X-ray Diffraction Studies of Lithium Intercalation in Li_xCoO_2. *J. Electrochem. Soc.* **1992**, *139*, 2091–2097. [CrossRef]

37. Shao-Horn, Y.; Levasseur, S.; Weill, F.; Delmas, C. Probing Lithium and Vacancy Ordering in O3 Layered Li_xCoO_2 ($x \approx 0.5$). *J. Electrochem. Soc.* **2003**, *150*, A366. [CrossRef]
38. Li, W.; Reimers, J.N.; Dahn, J.R. In situ x-ray diffraction and electrochemical studies of $Li_{1-x}NiO_2$. *Solid State Ion.* **1993**, *67*, 123–130. [CrossRef]
39. Peres, J.P.; Weill, F.; Delmas, C. Lithium/vacancy ordering in the monoclinic Li_xNiO_2 ($0.50 \leq x \leq 0.75$) solid solution. *Solid State Ion.* **1999**, *116*, 19–27. [CrossRef]
40. Arai, H.; Okada, S.; Ohtsuka, H.; Ichimura, M.; Yamaki, J. Characterization and cathode performance of $Li_{1-x}Ni_{1+x}O_2$ prepared with the excess lithium method. *Solid State Ion.* **1995**, *80*, 261–269. [CrossRef]
41. Kim, H.; Ji, H.; Wang, J.; Ceder, G. Next-Generation Cathode Materials for Non-aqueous Potassium-Ion Batteries. *Trends Chem.* **2019**, *1*, 682–692. [CrossRef]
42. Lee, W.; Kim, J.; Yun, S.; Choi, W.; Kim, H.; Yoon, W.-S. Multiscale factors in designing alkali-ion (Li, Na, and K) transition metal inorganic compounds for next-generation rechargeable batteries. *Energy Environ. Sci.* **2020**, *13*, 4406–4449. [CrossRef]
43. Tian, Y.; Zeng, G.; Rutt, A.; Shi, T.; Kim, H.; Wang, J.; Koettgen, J.; Sun, Y.; Ouyang, B.; Chen, T.; et al. Promises and Challenges of Next-Generation "Beyond Li-ion" Batteries for Electric Vehicles and Grid Decarbonization. *Chem. Rev.* **2021**, *121*, 1623–1669. [CrossRef] [PubMed]
44. Berthelot, R.; Carlier, D.; Delmas, C. Electrochemical investigation of the P2–Na_xCoO_2 phase diagram. *Nat. Mater.* **2011**, *10*, 74–80. [CrossRef] [PubMed]
45. Xu, J.; Lee, D.A.E.H.O.E.; Meng, Y.S. Recent advances in sodium intercalation positive electrode materials for sodium ion batteries. *Funct. Mater. Lett.* **2013**, *6*, 1330001. [CrossRef]
46. Hironaka, Y.; Kubota, K.; Komaba, S. P2- and P3-K_xCoO_2 as an electrochemical potassium intercalation host. *Chem. Commun.* **2017**, *53*, 3693–3696. [CrossRef] [PubMed]
47. Kim, H.; Kim, J.C.; Bo, S.-H.; Shi, T.; Kwon, D.-H.; Ceder, G. K-Ion Batteries Based on a P2-Type $K_{0.6}CoO_2$ Cathode. *Adv. Energy Mater.* **2017**, *7*, 1700098. [CrossRef]
48. Sun, Y.-K.; Han, J.-M.; Myung, S.-T.; Lee, S.-W.; Amine, K. Significant improvement of high voltage cycling behavior AlF_3-coated $LiCoO_2$ cathode. *Electrochem. Commun.* **2006**, *8*, 821–826. [CrossRef]
49. Radin, M.D.; Van der Ven, A. Stability of Prismatic and Octahedral Coordination in Layered Oxides and Sulfides Intercalated with Alkali and Alkaline-Earth Metals. *Chem. Mater.* **2016**, *28*, 7898–7904. [CrossRef]
50. DeKock, R.L.; Gray, H.B. *Chemical Structure and Bonding*; The Benjamin/Cummings Publishing Company: Menlo Park, CA, USA, 1980.
51. Sun, J.; Ruzsinszky, A.; Perdew, J.P. Strongly Constrained and Appropriately Normed Semilocal Density Functional. *Phys. Rev. Lett.* **2015**, *115*, 36402. [CrossRef]
52. Aydinol, M.K.; Kohan, A.F.; Ceder, G.; Cho, K.; Joannopoulos, J. Ab initio study of lithium intercalation in metal oxides and metal dichalcogenides. *Phys. Rev. B* **1997**, *56*, 1354–1365. [CrossRef]
53. Marianetti, C.A.; Morgan, D.; Ceder, G. First-principles investigation of the cooperative Jahn-Teller effect for octahedrally coordinated transition-metal ions. *Phys. Rev. B* **2001**, *63*, 224304. [CrossRef]
54. Akimoto, J.; Gotoh, Y.; Oosawa, Y. Synthesis and Structure Refinement of $LiCoO_2$ Single Crystals. *J. Solid State Chem.* **1998**, *141*, 298–302. [CrossRef]
55. Wolverton, C.; Zunger, A. First-Principles Prediction of Vacancy Order-Disorder and Intercalation Battery Voltages in $LiCoO_2$. *Phys. Rev. Lett.* **1998**, *81*, 606–609. [CrossRef]
56. Yin, S.-C.; Rho, Y.-H.; Swainson, I.; Nazar, L.F. X-ray/Neutron Diffraction and Electrochemical Studies of Lithium De/Re-Intercalation in $Li_{1-x}Co_{1/3}Ni_{1/3}Mn_{1/3}O_2$ ($x = 0 \rightarrow 1$). *Chem. Mater.* **2006**, *18*, 1901–1910. [CrossRef]
57. Reed, J.; Ceder, G. Role of Electronic Structure in the Susceptibility of Metastable Transition-Metal Oxide Structures to Transformation. *Chem. Rev.* **2004**, *104*, 4513–4534. [CrossRef] [PubMed]
58. Park, H.-S.; Hwang, S.-J.; Choy, J.-H. Relationship between Chemical Bonding Character and Electrochemical Performance in Nickel-Substituted Lithium Manganese Oxides. *J. Phys. Chem. B* **2001**, *105*, 4860–4866. [CrossRef]
59. Chernova, N.A.; Roppolo, M.; Dillon, A.C.; Whittingham, M.S. Layered vanadium and molybdenum oxides: Batteries and electrochromics. *J. Mater. Chem.* **2009**, *19*, 2526–2552. [CrossRef]
60. Radin, M.D.; Vinckeviciute, J.; Seshadri, R.; Van der Ven, A. Manganese oxidation as the origin of the anomalous capacity of Mn-containing Li-excess cathode materials. *Nat. Energy* **2019**, *4*, 639–646. [CrossRef]
61. Vinckeviciute, J.; Kitchaev, D.A.; Van der Ven, A. A Two-Step Oxidation Mechanism Controlled by Mn Migration Explains the First-Cycle Activation Behavior of Li_2MnO_3-Based Li-Excess Materials. *Chem. Mater.* **2021**, *33*, 1625–1636. [CrossRef]
62. Olivetti, E.A.; Ceder, G.; Gaustad, G.G.; Fu, X. Lithium-Ion Battery Supply Chain Considerations: Analysis of Potential Bottlenecks in Critical Metals. *Joule* **2017**, *1*, 229–243. [CrossRef]
63. Van der Ven, A. Lithium Diffusion in Layered Li_xCoO_2. *Electrochem. Solid-State Lett.* **1999**, *3*, 301. [CrossRef]
64. Xia, H.; Lu, L.; Ceder, G. Substrate effect on the microstructure and electrochemical properties of $LiCoO_2$ thin films grown by PLD. *J. Alloys Compd.* **2006**, *417*, 304–310. [CrossRef]
65. Jang, Y.-I.; Neudecker, B.J.; Dudney, N. Lithium diffusion in Li_xCoO_2 ($0.45 < x < 0.7$) Intercalation cathodes. *Electrochem. Solid-State Lett.* **2001**, *4*, A74. [CrossRef]

66. Ohzuku, T.; Ueda, A. Solid-State Redox Reactions of $LiCoO_2$ (R3m) for 4 Volt Secondary Lithium Cells. *J. Electrochem. Soc.* **1994**, *141*, 2972–2977. [CrossRef]
67. Amatucci, G.G.; Tarascon, J.M.; Klein, L.C. CoO_2, the End Member of the Li_xCoO_2 Solid Solution. *J. Electrochem. Soc.* **1996**, *143*, 1114–1123. [CrossRef]
68. Van der Ven, A.; Aydinol, M.K.; Ceder, G. First-Principles Evidence for Stage Ordering in Li_xCoO_2. *J. Electrochem. Soc.* **1998**, *145*, 2149–2155. [CrossRef]
69. Van der Ven, A.; Ceder, G. Lithium diffusion mechanisms in layered intercalation compounds. *J. Power Sources* **2001**, *97–98*, 529–531. [CrossRef]
70. Urban, A.; Lee, J.; Ceder, G. The Configurational Space of Rocksalt-Type Oxides for High-Capacity Lithium Battery Electrodes. *Adv. Energy Mater.* **2014**, *4*, 1400478. [CrossRef]
71. Van der Ven, A.; Bhattacharya, J.; Belak, A.A. Understanding Li Diffusion in Li-Intercalation Compounds. *Acc. Chem. Res.* **2013**, *46*, 1216–1225. [CrossRef] [PubMed]
72. Kang, K.; Ceder, G. Factors that affect Li mobility in layered lithium transition metal oxides. *Phys. Rev. B* **2006**, *74*, 94105. [CrossRef]
73. Kang, K.; Meng, Y.S.; Bréger, J.; Grey, C.P.; Ceder, G. Electrodes with High Power and High Capacity for Rechargeable Lithium Batteries. *Science* **2006**, *311*, 977–980. [CrossRef]
74. Lee, J.; Urban, A.; Li, X.; Su, D.; Hautier, G.; Ceder, G. Unlocking the Potential of Cation-Disordered Oxides for Rechargeable Lithium Batteries. *Science* **2014**, *343*, 519–522. [CrossRef]
75. Ji, H.; Urban, A.; Kitchaev, D.A.; Kwon, D.-H.; Artrith, N.; Ophus, C.; Huang, W.; Cai, Z.; Shi, T.; Kim, J.C.; et al. Hidden structural and chemical order controls lithium transport in cation-disordered oxides for rechargeable batteries. *Nat. Commun.* **2019**, *10*, 592. [CrossRef]
76. Lun, Z.; Ouyang, B.; Kwon, D.-H.; Ha, Y.; Foley, E.E.; Huang, T.-Y.; Cai, Z.; Kim, H.; Balasubramanian, M.; Sun, Y.; et al. Cation-disordered rocksalt-type high-entropy cathodes for Li-ion batteries. *Nat. Mater.* **2021**, *20*, 214–221. [CrossRef]
77. Clément, R.J.; Lun, Z.; Ceder, G. Cation-disordered rocksalt transition metal oxides and oxyfluorides for high energy lithium-ion cathodes. *Energy Environ. Sci.* **2020**, *13*, 345–373. [CrossRef]
78. Baur, C.; Källquist, I.; Chable, J.; Chang, J.H.; Johnsen, R.E.; Ruiz-Zepeda, F.; Mba, J.M.A.; Naylor, A.J.; Garcia-Lastra, J.M.; Vegge, T.; et al. Improved cycling stability in high-capacity Li-rich vanadium containing disordered rock salt oxyfluoride cathodes. *J. Mater. Chem. A* **2019**, *7*, 21244–21253. [CrossRef]
79. Chen, R.; Ren, S.; Yavuz, M.; Guda, A.A.; Shapovalov, V.; Witter, R.; Fichtner, M.; Hahn, H. Li^+ intercalation in isostructural Li_2VO_3 and Li_2VO_2F with $O2^-$ and mixed $O2^-/F^-$ anions. *Phys. Chem. Chem. Phys.* **2015**, *17*, 17288–17295. [CrossRef]
80. Lee, J.; Kitchaev, D.A.; Kwon, D.-H.; Lee, C.-W.; Papp, J.K.; Liu, Y.-S.; Lun, Z.; Clement, R.J.; Shi, T.; McCloskey, B.D.; et al. Reversible Mn^{2+}/Mn^{4+} double redox in lithium-excess cathode materials. *Nature* **2018**, *556*, 185–190. [CrossRef]
81. Takeda, N.; Hoshino, S.; Xie, L.; Chen, S.; Ikeuchi, I.; Natsui, R.; Nakura, K.; Yabuuchi, N. Reversible Li storage for nanosize cation/anion-disordered rocksalt-type oxyfluorides: $LiMoO_{2-x}$ LiF ($0 \leq x \leq 2$) binary system. *J. Power Sources* **2017**, *367*, 122–129. [CrossRef]
82. Glazier, S.L.; Li, J.; Zhou, J.; Bond, T.; Dahn, J.R. Characterization of Disordered $Li_{(1+x)}Ti_{2x}Fe_{(1-3x)}O2$ as Positive Electrode Materials in Li-Ion Batteries Using Percolation Theory. *Chem. Mater.* **2015**, *27*, 7751–7756. [CrossRef]
83. Cambaz, M.A.; Vinayan, B.P.; Euchner, H.; Pervez, S.A.; Geßwein, H.; Braun, T.; Gross, A.; Fichtner, M. Design and Tuning of the Electrochemical Properties of Vanadium-Based Cation-Disordered Rock-Salt Oxide Positive Electrode Material for Lithium-Ion Batteries. *ACS Appl. Mater. Interfaces* **2019**, *11*, 39848–39858. [CrossRef] [PubMed]
84. Urban, A.; Abdellahi, A.; Dacek, S.; Artrith, N.; Ceder, G. Electronic-Structure Origin of Cation Disorder in Transition-Metal Oxides. *Phys. Rev. Lett.* **2017**, *119*, 176402. [CrossRef] [PubMed]
85. Lun, Z.; Ouyang, B.; Kitchaev, D.A.; Clément, R.J.; Papp, J.K.; Balasubramanian, M.; Ceder, G. Improved Cycling Performance of Li-Excess Cation-Disordered Cathode Materials upon Fluorine Substitution. *Adv. Energy Mater.* **2019**, *9*, 1802959. [CrossRef]